Convective Velocity Reversal Caused by Turbulence Transition in Tokamak Plasma

W. L. Zhong,[1] X. L. Zou,[2,*] C. Bourdelle,[2] S. D. Song,[1] J. F. Artaud,[2] T. Aniel,[2] and X. R. Duan[1]
[1]Southwestern Institute of Physics, P.O. Box 432, Chengdu 610041, People's Republic of China
[2]CEA, IRFM, F-13108 Saint-Paul-lez-Durance, France
(Received 16 January 2013; published 26 December 2013)

Particle transport has been studied in the Tore Supra tokamak by using modulated ion cyclotron resonance heating to generate perturbations of density and temperature. For the first time, a reversal of the particle convective velocity and a strong increase in the turbulent particle flux have been clearly observed. When the mixed critical gradient $\zeta_c = R/L_T + 4(R/L_n) = 22$ is exceeded, the particle flux increases sharply and the convective velocity reverses from inward to outward. These observations are in agreement with quasilinear, gyrokinetic calculations. The critical gradient corresponds to a transition from an instability driven by the ion temperature gradient to the onset of another instability caused by trapped electrons.

DOI: 10.1103/PhysRevLett.111.265001 PACS numbers: 52.25.Fi, 52.35.Ra, 52.55.Fa, 52.65.Tt

Particle transport is a key issue in magnetized fusion plasmas. Understanding its mechanism is essential for the design of future fusion reactors [1]. Experiments in tokamaks show that, in addition to transport from binary collisions (neoclassical transport), small-scale turbulence due to instabilities (so-called anomalous transport) plays an important role in both particle and heat transport. Theoretical work has identified thresholds for density and/or temperature gradients at which the ion temperature gradient (ITG) mode and trapped electron mode (TEM) are destabilized [2]. In tokamaks, particle convection driven by the ITG is always inward, while particle convection driven by TEM can be outward via the thermodiffusion term [2]. This difference is used in present experiments for identifying the turbulence modes. It has been experimentally demonstrated that the particle convective velocity is turbulent and much larger than the value predicted by the collisional neoclassical theory [3]. In the steady state and without a central particle source, the particle transport can be characterized by the density peaking factor. Indeed, this parameter can be directly linked to the ratio between the inward convective velocity V and the outward particle diffusivity D. As shown in JET and ASDEX-U, the density peaking factor decreases with increasing collisionality [1,4]. However, measurements made in steady state conditions cannot determine unique values for V and D, but a perturbation experiment can be an effective way to do this [5,6]. In HL-2A, a spontaneous particle transport barrier has been evidenced in experiments with supersonic molecular beam injection [7]. In Tore Supra, ion cyclotron resonance heating (ICRH) modulations in the minority heating scenario have been used to investigate particle transport. Experimental results and the comparison with a quasilinear gyrokinetic turbulent transport model [8] are reported in this Letter.

The plasma parameters in the present experiments are the following: major radius $R = 2.4$ m, minor radius $a = 0.72$ m, magnetic field $B_0 = 3.3$ T, and plasma current $I_p = 1.0$ MA. The ICRH launched power is about 2 MW, and the ICRH power is modulated at 1 Hz with a duty cycle of 50%. Only L-mode plasmas with ICRH are considered in this work.

Figure 1 shows the time evolution of the main parameters of a typical discharge with ICRH modulation. The electron temperature is measured by an electron cyclotron emission radiometer. The line-averaged density is measured by a far infrared interferometer. As shown in Fig. 1, the central electron temperature T_{e0}, the line-averaged electron density n_{el}, and the stored energy W_{dia} are modulated by the ICRH power. All these modulations are in phase with the ICRH modulation. During the ICRH phase, no new magnetohydrodynamics instability is observed, except that the sawteeth become larger. It should be noted that the density perturbation is likely to be generated by an influx of gas due to the additional heating of the boundary with ICRH. The electron density profile is measured by two

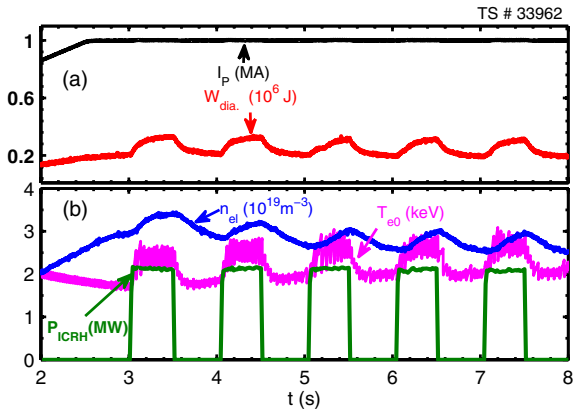

FIG. 1 (color online). Typical discharge with ICRH modulation. (a) Time evolution of the plasma current I_P and the stored energy W_{dia}. (b) Time evolution of the line-averaged electron density n_{el}, the central electron temperature T_{e0}, and the ICRH power P_{ICRH}.

X-mode reflectometers with high resolution in time and space [9].

Figure 2(a) shows the time evolution of the electron densities at different radii. Figure 2(b) displays the 2D image of the density perturbation response to a single ICRH pulse with $\Delta n_e(r/a,t) = n_e(r/a,t) - n_e(r/a,t_0)$, where t_0 is the starting time for ICRH. From this figure, it is clear that the density perturbation starts at the last closed flux surface (LCFS) and then propagates inward. The particle source can be estimated by $S(r/a,t) = \partial n_e/\partial t$, when the time interval ∂t is short enough from the starting time t_0, at which the particle transport process is negligible. Figure 2(c) illustrates the radial profile of this source generated by ICRH, located just outside of the LCFS. The particle source width is estimated to be 2.2 cm.

The amplitude (A_ω) and the phase (ϕ_ω) of the first harmonic of the Fourier transform of the modulated density are shown in Figs. 3(a) and 3(b). As shown in Ref. [6], the phase depends mainly on the diffusivity D and weakly on the convective velocity V, while the amplitude depends strongly on both V and D. By exploiting these different sensitivities, the values of V and D can be separately determined by fitting the experimental data of A_ω and ϕ_ω with an analytical linear transport model [10]. For the simulation and according to the sharp change in the amplitude and phase, four zones have been identified as indicated in Table I. Zone V ($1.0 < r/a < 1.14$) corresponding to the scrape-off layer is not considered here, since perpendicular transport is not the dominant physical process in this zone, and consequently the perturbation analysis is not valid. Before the simulation, interesting information could be directly deduced from the figures. As the location of the particle perturbation source is given by the minimum of the phase, from Fig. 3(b) this particle source should be located close to the LCFS, which is consistent with that shown in Fig. 2(c). As the maximum of the amplitude located at $r/a = 0.95$ is shifted inward relative to the particle source position, this unambiguously indicates the presence of a strong inward pinch velocity inside zone IV. As the diffusivity D is inversely proportional to the square of the derivative of the phase, the fact that the phase gradient undergoes a sharp change at $r/a = 0.52$ shows a jump in D or a transport barrier at this position. In the slab geometry approximation, the sign of the convective velocity is given by that of $\nabla A_\omega + \nabla\phi_\omega$. Thus the convective velocity should be inward in region I and outward in regions II and III. As shown in Figs. 3(a) and 3(b), the best fit (solid line) has been found with the optimized D and V plotted in Fig. 3(c). The values of D and V are given in Table I. V is negative for inward and positive for outward convection. The results of the simulation confirm the previous observations. It should be emphasized that the edge particle pinch (-10 m/s) in zone IV plays a crucial role for the fueling. It is important to note that all these results are obtained for the transient phase and are not valid for the steady state. Indeed, numerous perturbation experiments have shown that the transient diffusivity is different and often higher than that of the steady state [11]. In the present case, the loop voltage is 0.7–0.9 V, and the Ware pinch is 0.03 m/s, much lower than that given in Table I.

The turbulence theory suggests that the key parameters for changes in transport processes are the normalized density gradient $R/L_n = -R\nabla n_e/n_e$ and the normalized temperature gradient $R/L_T = -R\nabla T_e/T_e$, and these parameters should be related to the sudden change in transport at the boundary between zones I and II. The values of R/L_n and R/L_T are lower in zone I (respectively, 3.1 and 8) than in zone II (respectively, 3.7 and 9), showing that the density and temperature gradients have a strong effect on D and V. Thus the plasma may be divided into three

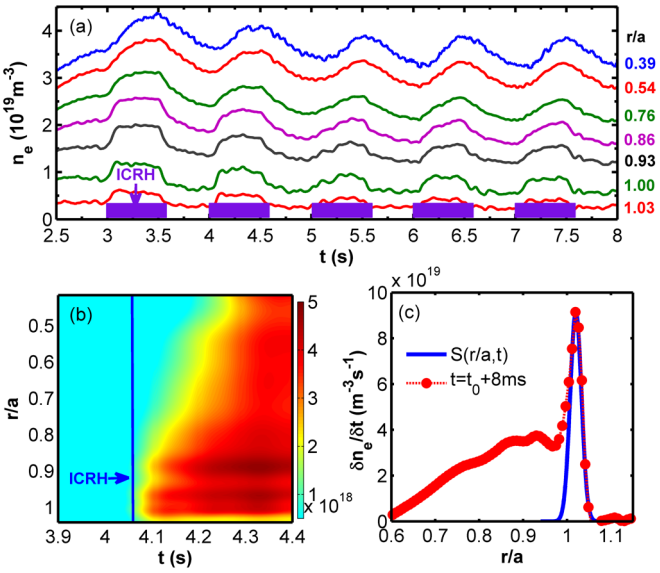

FIG. 2 (color online). (a) Time evolution of the electron density modulated by 1 Hz ICRH, at different radii. (b) 2D image of the density perturbation response to one ICRH pulse. (c) Particle source profile deposited by the ICRH at $t_0 = 3.075$ s. The particle source $S(r/a,t)$ is fitted by a Gaussian function.

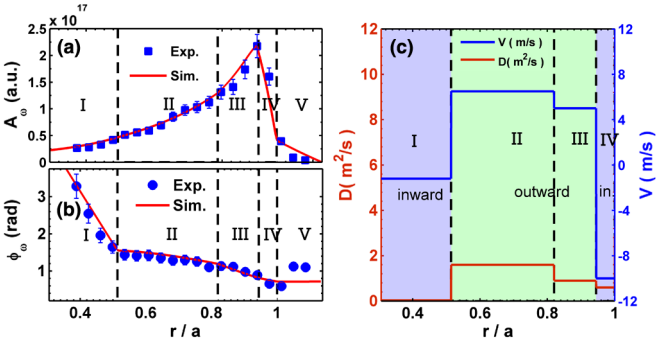

FIG. 3 (color online). Amplitude (a) and the phase (b) of the Fourier transform of the density modulated by ICRH. The solid lines represent the simulation with an analytical transport model using the values of D and V given in (c), with positive V for outward convection and negative V for inward convection.

TABLE I. Values of D and V plotted in Fig. 3(c) for different zones.

	Zone I $0.3 < r/a < 0.52$	Zone II $0.52 < r/a < 0.82$	Zone III $0.82 < r/a < 0.95$	Zone IV $0.95 < r/a < 1$
D (m^2/s)	0.03 ± 0.01	1.6 ± 0.1	0.9 ± 0.1	0.6 ± 0.15
V (m/s)	-1.2 ± 0.03	6.5 ± 1.5	5 ± 1	-10 ± 2

parts: the low gradient region (inward pinch) with zone I, the high gradient region (outward convection) including zones II and III, and the fueling region, i.e., zone IV.

To study the effect of the density and temperature gradient on particle transport, a series of five discharges with line-averaged densities varying from 2.2×10^{19} to 4×10^{19} m^{-3} have been performed and analyzed in Tore Supra. R/L_n and R/L_T are calculated by averaging over the modulation periods. In these modulation experiments, R/L_n varies from 2.1 to 4.0, and R/L_T varies from 7.8 to 9.4.

Figure 4 shows the dependences of the diffusive particle flux, defined by $\Gamma_D = -D\nabla n_e$, and the convective velocity V on R/L_T at $r/a = 0.5$ at $r/a = 0.5$ and $r/a = 0.6$ illustrated by different symbols. One can notice that the particle flux increases steeply when R/L_T exceeds a threshold. Analogous to the diffusive particle flux, the convective velocity changes direction from inward to outward when the same threshold is exceeded. This threshold is estimated roughly to be $(R/L_T)_{\text{crit}} \approx 8.5$.

The dependences of Γ_D and V on R/L_n are shown in Fig. 5. A critical density gradient is also clearly observed for both diffusive flux and convective velocity. The critical value is about $(R/L_n)_{\text{crit}} \approx 3.3$. Beyond the threshold, Γ_D increases sharply with R/L_n [Fig. 5(a)]. For $R/L_n < 3.3$, the convective velocity V is inward and nearly -1 m/s, as shown in Fig. 5(b). For $R/L_n > 3.3$, the convective velocity is outward and the outward convection strongly increases with R/L_n. It is interesting to note that most of the data points in Fig. 4 over the R/L_T threshold are the same points that are over the R/L_n threshold in Fig. 5, with the exception of the point at $R/L_T = 8.2$, $\Gamma_D = 1.8 \times 10^{19}$ $m^2\,s^{-1}$, and $V = 0.3$ m/s, which corresponds to a larger R/L_n exceeding the threshold. This suggests first that the two critical gradients are likely interdependent and second that the dependence on R/L_n is the dominant one. This could be the result of a feedback loop, as discussed later.

The above experimental observations can be compared to numerical simulations carried out with the quasilinear gyrokinetic code QUALIKIZ [12]. Figure 6(a) shows the turbulence stability diagram obtained with QUALIKIZ, which is computed on a single wave number corresponding to the maximum of the linear ITG-TEM spectrum. The relevant parameters used in this simulation are obtained from the modulation discharge. The instability thresholds are identified within the interval of the density and temperature gradient values where the linear growth rates of the unstable modes become nonzero. We can see from this figure that the points corresponding to the inward convection (red circles) are located in the area where only ITG is unstable, while the points corresponding to the outward convection (blue diamonds) are located in the area where both ITG and TEM are unstable. Thus the inward and outward convection points are separated by the TEM threshold boundary.

By fitting the TEM threshold boundary with a straight line, a mixed critical gradient is given by $\zeta_c = R/L_T + 4(R/L_n) = 22$ as shown in Fig. 6(a). Figures 6(b) and 6(c) plot, respectively, the diffusive flux and convective velocity as functions of the new variable $\zeta = R/L_T + 4(R/L_n)$. Both the strong diffusive flux increase and the convective velocity direction reversal occur when the variable ζ exceeds the threshold $\zeta_c = 22$. This indicates that the density and temperature gradients in the steady state should be very close to the boundary of the TEM threshold. This suggests that the

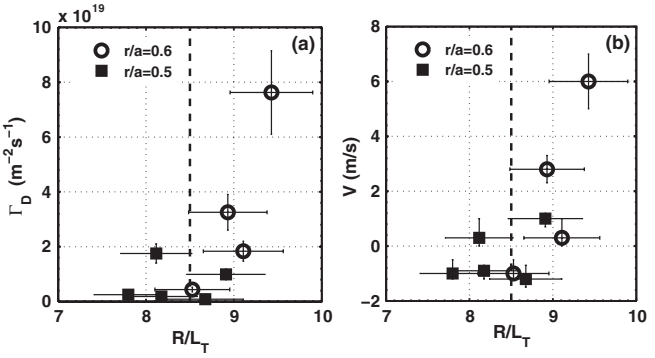

FIG. 4. (a) Diffusive particle flux and (b) convective velocity vs the normalized temperature gradient. The critical temperature gradient is 8.5.

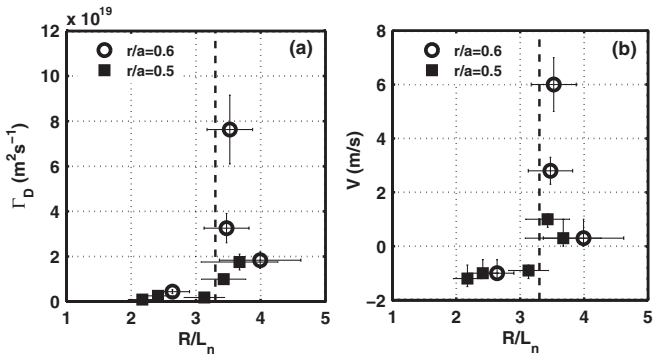

FIG. 5. (a) Diffusive flux and (b) convective velocity vs the normalized electron density gradient. The critical density gradient is 3.3.

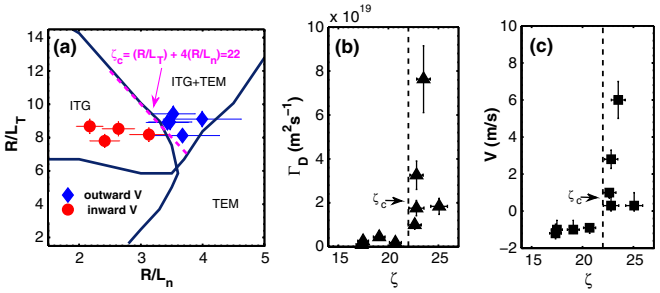

FIG. 6 (color online). (a) Turbulence stability diagram with QUALIKIZ model. The ITG-TEM boundary is fitted with the line of $\zeta_c = R/L_T + 4(R/L_n) = 22$, which is the mixed critical gradient including the electron density and temperature gradients. (b) Diffusive particle flux vs ζ. (c) Convective velocity vs ζ.

behavior of the density profile is governed by a feedback loop, as a self-regulating system. When the density gradient is low, only the ITG exists, which induces an additional thermodiffusion inward particle pinch leading to a density gradient increase. The density gradient increases until it exceeds the threshold by triggering the TEM, which leads to an outward thermodiffusive particle convection. In return, this action causes a density gradient decrease. When the density gradient goes below the threshold again, the TEM disappears, and only the ITG remains, and so on. This mechanism can explain the density profile stiffness observed in tokamaks. In the steady state and in the core of the plasma, the inward particle convection is balanced by the outward diffusive flux. This suggests that the reversal of thermodiffusion might be the mechanism explaining the experimental observations. It should be noted that the curvature-driven pinch [2] remains nearly constant in the present experiments and is dominated by the thermodiffusion term.

Results of perturbation transport experiments with ICRH modulation in the Tore Supra tokamak show that, when the mixed critical gradient $\zeta_c = R/L_T + 4(R/L_n) = 22$ is exceeded, the diffusive flux increases sharply, and the particle convective velocity direction is reversed from inward to outward. Agreement between the experimental results and the quasilinear gyrokinetic simulation is qualitatively satisfactory. It demonstrates that the strong diffusive flux increase and the convective velocity direction reversal correspond to the ITG-TEM transition.

This work is supported within the framework of the cooperation between the French Commissariat à l'Energie Atomique et aux Energies Alternatives (CEA) and the China National Nuclear Corporation (CNNC). One of the authors, W. L. Z., thanks Y. Buravand and J. Citrin for their help in providing access to QUALIKIZ and running the simulation.

*Corresponding author.
xiao-lan.zou@cea.fr

[1] H. Weisen *et al.*, Nucl. Fusion **45**, L1 (2005).
[2] X. Garbet, L. Garzotti, P. Mantica, H. Nordman, M. Valovic, H. Weisen, and C. Angioni, Phys. Rev. Lett. **91**, 035001 (2003).
[3] G. T. Hoang, C. Bourdelle, X. Garbet, G. Giruzzi, T. Aniel, M. Ottaviani, W. Horton, P. Zhu, and R. V. Budny, Phys. Rev. Lett. **87**, 125001 (2001).
[4] C. Angioni, A. G. Peeters, G. V. Pereverzev, F. Ryter, G. Tardini, and ASDEX Upgrade Team, Phys. Rev. Lett. **90**, 205003 (2003).
[5] W. W. Xiao *et al.*, Rev. Sci. Instrum. **81**, 013506 (2010).
[6] K. W. Gentle, O. Gehre, and K. Krieger, Nucl. Fusion **32**, 217 (1992).
[7] W. W. Xiao *et al.*, Phys. Rev. Lett. **104**, 215001 (2010).
[8] A. Casati *et al.*, Nucl. Fusion **49**, 085012 (2009).
[9] F. Clairet, C. Bottereau, J. M. Chareau, M. Paume, and R. Sabot, Plasma Phys. Controlled Fusion **43**, 429 (2001).
[10] S. P. Eury, E. Harauchamps, X. L. Zou, and G. Giruzzi, Phys. Plasmas **12**, 102511 (2005).
[11] S. D. Song *et al.*, Nucl. Fusion **52**, 033006 (2012).
[12] C. Bourdelle, X. Garbet, F. Imbeaux, A. Casati, N. Dubuit, R. Guirlet, and T. Parisot, Phys. Plasmas **14**, 112501 (2007).